Theory of intensities in inelastic-electron tunneling spectroscopy orientation of adsorbed molecules

John Kirtley

IBM Thomas J. Watson Research Center, Yorktown Heights, New York 10598

James T. Hall

National Bureau of Standards, Washington, D.C. 20234
(Received 14 November 1979)

A dipole-potential, transfer Hamiltonian theory of intensities is applied to the tunneling spectrum of $CH_3SO_3{}^-$ chemisorbed on alumina. In a previous study of the vibrational energies of this molecule, Hall and Hansma proposed that it absorbed on alumina with the C–S bond oriented normal to the surface. Comparison of the predictions of the present theory with experiment supports this orientation. Dipole derivatives generated from tunneling intensities compare well with those obtained from infrared measurements for similar species.

INTRODUCTION

An understanding of intensities in inelastic-electron tunneling spectroscopy (IETS)[1,2] may enable one to infer the orientation and possibly other properties of molecules adsorbed on surfaces. To date, no theoretical model for intensities in IETS has been compared with experiment for complex molecules. We develop here a dipole-potential transfer Hamiltonian theory of intensities in IETS to the point where it is possible to carry out such a detailed comparison.

We apply this theory to the spectrum of methanesulfonate ($CH_3SO_3{}^-$) on alumina. Kirtley, Scalapino, and Hansma[3] have shown using this theory that vibrations with net dipole moments normal to the surface have larger intensities than vibrations with net dipole moments parallel to the surface when image charge effects are taken into account. We will show that this orientation "selection rule" depends sensitively on the distance of the image plane to the origin of the dipole potential. Reasonable choices for the molecule-image plane distance and for dipole derivatives from infrared measurements lead to theoretical intensities that agree reasonably well with experiment if the C–S bond is assumed to be normal to the surface. Our intensity theory, therefore, supports the orientation proposed for $CH_3SO_3{}^-$ by Hall and Hansma[4] from a consideration of vibrational mode frequencies.

In IETS the vibrational spectrum of a molecular monolayer or submonolayer in a metal-metal oxide-molecular layer-metal tunneling junction appears as small peaks in the second derivative of the current-voltage characteristic of the junction. These peaks are the result of small increases in the tunneling conduction across the junction due to inelastic tunneling processes: Tunneling electrons lose energy $\hbar\omega$ to the excitation of a molecular vibration in the barrier region. The voltages of the peaks are given at low temperatures (spectra are run at or below 4.2 K) by the quantum relation $eV = \hbar\omega$, where V is the bias voltage across the tunneling barrier. Our object is to calculate the magnitudes of the conduction increases due to inelastic tunneling processes.

Since the basic framework of the theory to be developed has been presented previously,[3] we will merely outline it here. We will assume that the oxide and molecular monolayer make up a simple square potential barrier of height ϕ (measured relative to the bottom of the conduction bond of metal 1) and width l. In some cases (especially for low effective molecular barrier heights[5]) it can be important to take into account the difference between the barrier heights of the oxide layer and the molecular monolayer. The difference in barrier heights is not expected to be important for $CH_3SO_3{}^-$ on alumina.

Following Bardeen's transfer Hamiltonian approach, the initial and final WKB approximation of free-electron-like wave functions localized on opposite sides of the barrier are given within the barrier by

$$\psi_i = \frac{1}{\sqrt{2}\,L^{3/2}} \frac{k_z^{1/2}}{K_z^{1/2}} e^{-K_z(s-z)} e^{i(k_x x + k_y y)} , \tag{1}$$

$$\psi_f = \frac{1}{\sqrt{2}\,L^{3/2}} \frac{k_z'^{1/2}}{K_z'^{1/2}} e^{-K_z' z} e^{i(k_x' x + k_y' y)} , \tag{2}$$

where

$$K_z = \left(\frac{2m}{\hbar^2}(\phi - E_z)\right)^{1/2} , \tag{3}$$

$$E_z = E - (\hbar^2/2m)(k_x^2 + k_y^2) \tag{4}$$

with similar relations for the final state (primed) parameters, E is the electron energy relative to the bottom of the conduction band, and L is an

arbitrary normalization length which will cancel out.

Electrons are transferred inelastically between the initial and final states by an interaction potential which we assume to be of the form

$$V_I(\vec{r},\vec{R}) = \sum_n \frac{-e^2 Z_n}{|\vec{r}-\vec{R}_n|} , \qquad (5)$$

where $\vec{r}$ is the position of the tunneling electron, $Z_n e$ is a partial charge localized at an atomic position $\vec{R}_n = a_n \hat{z} + b_n \hat{x} + c_n \hat{y}$, and the sum n is over all atoms in the molecule. In principle, this sum could be made over all spatial positions with a small mesh to take into account the detailed molecular-bond charge distributions. In practice, experimental evidence[6] points toward a relatively long-range potential, so that (1) an atom-by-atom sum is sufficient, and (2) our neglect of exchange is justifiable.

The component of the total potential (5) which transfers electrons inelastically is that which os-

cillates at the vibrational mode frequency. If we take the picture of static charges attached to the vibrating atoms, the interaction potential becomes in the harmonic approximation,

$$V_i^k(\vec{r},\vec{R}) = \sum_n -e^2 Z_n^k \delta\vec{R}_n^k \cdot \vec{\nabla}_n\left(\frac{1}{|\vec{r}-\vec{R}_n^0|}\right)e^{i\omega_k t} , \quad (6)$$

where $\vec{R}_n^0$ and $\delta\vec{R}_n^k$ are, respectively, the equilibrium position and vibrational amplitude for the nth atom due to the kth normal mode of the molecule. This potential has the form of a sum of dipole potentials, each dipole located on an atom in the molecule

$$V_i^k(\vec{r},\vec{R}) = \sum_n -\vec{\mu}_n^k \cdot \vec{\nabla}_n\left(\frac{1}{|\vec{r}-\vec{R}_n^0|}\right)e^{i\omega_k t} , \qquad (7)$$

$$\vec{\mu}_n^k = e Z_n^k \delta\vec{R}_n^k . \qquad (8)$$

If we include the images of the oscillating charges in the two metal surfaces and dielectric screening in the oxide, the potential becomes

$$V_i^k(\vec{r},\vec{R}) = \sum_{p=-\infty}^{\infty} \sum_n \frac{-e}{\epsilon}\vec{\mu}_n^k \cdot \vec{\nabla}_n$$
$$\times\left(\frac{1}{|\vec{r}-\vec{R}_n-2ps\hat{z}|} - \frac{1}{|\vec{r}-\vec{R}_n-(2ps-2a_n)\hat{z}|}\right) , \qquad (9)$$

where ϵ is the dielectric constant of the oxide (taken to be 3 for Al_2O_3).

Fermi's Golden Rule for the transition rate between initial and final states on opposite sides of the tunneling barrier becomes

$$\omega_{if}^k = (2\pi/\hbar)|M_{if}^k|^2 \delta(\epsilon_i - \epsilon_f - \hbar\omega_k) , \qquad (10)$$

where ϵ_i, ϵ_f are the initial- and final-state electron energies, and δ is the Dirac delta function. The matrix element M_{if}^k is defined as

$$M_{if}^k = \int_0^l d^3x\, \psi_f^* V_i^k(\vec{r},\vec{R})\psi_i \qquad (11)$$

with ψ_i, ψ_f given by Eqs. (1) and (2), and $V_i^k(\vec{r},\vec{R})$ given by Eq. (9). By Fourier transforming the potential and performing the required integrations, we can evaluate the matrix element

$$M_{if}^k = \frac{\pi e}{\epsilon L^3}\sum_{nl}\langle\mu_n^{kl}\rangle e^{i\alpha_x b_n}e^{i\alpha_y c_n}g_n^{kl} , \qquad (12)$$

$$g_n^{kl} = \xi_z e^{-K_z s}\frac{\alpha_l}{\alpha_\perp}\left[\frac{e^{\alpha_\perp a_n} \pm e^{-\alpha_\perp a_n}}{e^{2s\alpha_\perp}-1}\left(\frac{e^{(\alpha_z-\alpha_\perp)s}-1}{\alpha_\perp-\alpha_z} + \frac{e^{(\alpha_z+\alpha_\perp)s}-1}{\alpha_\perp+\alpha_z}\right)\right.$$
$$\left. +\frac{1}{\alpha_\perp-\alpha_z}\left[e^{(\alpha_z-\alpha_\perp)s}(e^{\alpha_\perp a_n} \pm e^{-\alpha_\perp a_n}) - (e^{\alpha_z a_n} \pm e^{-\alpha_\perp a_n})\right] \pm \frac{1}{\alpha_\perp+\alpha_z}(e^{\alpha_z a_n} - e^{-\alpha_\perp a_n})\right] , \qquad (13)$$

where $\langle\mu_n^{kl}\rangle$ is the lth Cartesian component of the expectation value of the dipole moment operator between the ground and first excited vibrational states of the kth normal mode due to the nth oscillating charge,

$$\alpha_x = k_x - k_x' ,$$
$$\alpha_y = k_y - k_y' ,$$
$$\xi_z = (k_z k_z'/K_z K_z')^{1/2} ,$$
$$\alpha_\perp = (\alpha_x^2 + \alpha_y^2)^{1/2} ,$$
$$\qquad (14)$$

$$\alpha_l = \begin{cases} \alpha_x, & l=1 \ (\hat{x}) \\ \alpha_y, & l=2 \ (\hat{y}) \\ \alpha_\perp, & l=3 \ (\hat{z}) \end{cases} \qquad (15)$$

the upper sign is taken for $l=3$ ($\hat{z}$) and the lower sign is taken for $l=1,2$ ($\hat{x},\hat{y}$).

The second derivative of the current due to the kth vibrational mode of the molecule is given by[3]

$$\frac{d^2 j^k}{d(\mathrm{eV})^2} = \frac{8\pi n e}{\hbar}\left(\frac{L}{\pi}\right)^6\left(\frac{m}{\hbar^2}\right)^3 \sqrt{\epsilon_F}\,(\epsilon_F' - eV)^{1/2}$$

$$\times \int_0^{2\pi} d\phi \int_0^{2\pi} d\phi' \int_0^1 d(\cos\theta)$$

$$\times \int_0^1 d(\cos\theta')\,|M_{iF}^k|^2$$

$$\times \delta(\hbar\omega_k - eV), \quad (16)$$

where j is the current per unit area through the junction, n is the surface density per unit area of dopant molecules, $\epsilon_F(\epsilon_F')$ is the Fermi energy in the initial (final) electrode, and the matrix element is evaluated on the Fermi surfaces (assumed spherical) of the two metal electrodes. [Note: Eq. (16) corrects a minor error in Eq. (14) of Ref. 3.] By making the transformation

$$\phi_1 = \phi,$$
$$\phi_2 = \phi - \phi', \quad (17)$$

one integration over azimuthal angles can be done immediately:

$$\int_0^{2\pi} d\phi_1\,|M_{iF}^k|^2 = \frac{\pi^2 e^2}{\epsilon^2 L^6}\sum_{n,\,m,\,l,\,l'}\langle\alpha_{ll'}'\rangle_{nm}\langle\mu_n^{kl}\rangle\langle\mu_m^{kl}\rangle g_n^{kl}g_m^{kl'},$$
$$(18)$$

where

$$\langle\alpha_{11}\rangle_{nm} = 2\pi\left[\frac{b_{nm}^2}{\rho_{nm}^2}J_0(\alpha_\perp\rho_{nm}) - \left(\frac{b_{nm}^2 - c_{nm}^2}{\rho_{nm}^3\alpha_\perp}\right)J_1(\alpha_\perp\rho_{nm})\right],$$

$$\langle\alpha_{12}\rangle_{nm} = 2\pi\frac{b_{nm}c_{nm}}{\rho_{nm}^2}\left(J_0(\alpha_\perp\rho_{nm}) - \frac{2}{\alpha_\perp\rho_{nm}}J_1(\alpha_\perp\rho_{nm})\right)$$

$$= \langle\alpha_{21}\rangle_{nm},$$

$$\langle\alpha_{22}\rangle_{nm} = 2\pi\left(\frac{c_{nm}^2}{\rho_{nm}^2}J_0(\alpha_\perp\rho_{nm}) + \frac{(b_{nm}^2 - c_{nm}^2)}{\rho_{nm}^3\alpha_\perp}J_0(\alpha_\perp\rho_{nm})\right),$$
$$(19)$$

$$\langle\alpha_{13}\rangle_{nm} = \langle\alpha_{31}\rangle_{nm} = \langle\alpha_{32}\rangle_{nm} = \langle\alpha_{23}\rangle_{nm} = 0,$$

$$\langle\alpha_{33}\rangle_{nm} = 2\pi J_0(\alpha_\perp\rho_{nm}),$$

where $b_{nm} = b_n - b_m$, $c_{nm} = c_n - c_m$, $\rho_{nm} = (b_{nm}^2 + c_{nm}^2)^{1/2}$, and $J_0(x)$ is the Bessel function of the first kind for $\nu = 0$. In the special case $\rho_{nm} = 0$, Eqs. (19) reduce to

$$\langle\alpha_{11}\rangle_{nm} = \langle\alpha_{22}\rangle_{nm} = \pi,$$
$$\langle\alpha_{12}\rangle_{nm} = \langle\alpha_{21}\rangle_{nm} = 0, \quad (20)$$
$$\langle\alpha_{33}\rangle_{nm} = 2\pi.$$

The change in conductance due to the kth vibrational mode becomes

$$\Delta\left(\frac{dj^k}{d(\mathrm{eV})}\right) = \frac{8e^5 m^3 n}{\epsilon^2\hbar^7\pi^3}\sqrt{\epsilon_F}\,(\epsilon_F' - eV)^{1/2}$$

$$\times \sum_{n,\,m,\,l,\,l'}\langle\mu_n^{kl}\rangle\langle\mu_m^{kl}\rangle A_{n,\,m,\,l,\,l'}^k, \quad (21)$$

$$A_{n,\,m,\,l,\,l'}^k = \int_0^{2\pi} d\phi_2 \int_0^1 d(\cos\theta)$$

$$\times \int_0^1 d(\cos\theta')\langle\alpha_{ll'}\rangle_{nm}g_n^{kl}g_m^{kl'}.$$
$$(22)$$

The final three integrations over incoming and outgoing angles were done numerically to obtain the coefficients $A_{n,\,m,\,l,\,l'}^k$ for a given molecular geometry, barrier parameters, and vibrational energy. For this work we set $l = 15$ Å, $\phi = 12$ eV, $\epsilon_F = \epsilon_F' = 10$ eV, parameters typically used to model the current voltage characteristics of these junctions.[5] Our results do not depend strongly on these parameters. An appropriate dimensionless quantity that will be compared with experiment is

$$\Delta(dj^k/d(eV))/(dj_e/d(eV)_{\mathrm{ref}}),$$

the ratio of the change in conductance due to the opening of the kth inelastic channel, divided by the total conductance at a reference voltage where

$$\frac{dj_e}{d(eV)} = \frac{eK_z^0}{(2\pi)^2 l\hbar}e^{-2sK_z^0} \quad (23)$$

and

$$K_z^0 \equiv [(2m/\hbar^2)(\phi - \epsilon_F)]^{1/2}$$

are given by the same model barrier as used for the inelastic conductance calculations.

Kirtley, Scalapino, and Hansma[3] have shown previously that the model outlined above, when applied to diatomic molecules (OH⁻ and CO), gives approximately the absolute magnitudes for IETS intensities and the ratio of intensities for opposite bias voltage polarities. In addition, the theory predicts that Raman-active as well as infrared-active modes should be observable, even neglecting molecular polarizability. Finally, molecular vibrations with net dipole moments normal to the surface have larger inelastic cross sections than vibrations with net dipole moments parallel to the surface for dipoles close to one electrode. Physically the reason for the last is that near a metal surface, the image dipole adds to the potential of a dipole normal to the interface, but tends to cancel out the potential of a dipole parallel to the interface. For very long wavelength excitations (and only one metal surface) one would expect to see only vibrations with dipole moments normal to the interface. This is not the case, however, for dipoles deep within the tunneling barrier. First, as pointed out in Ref. 3, energy loss and off-axis scattering [resulting in nonzero α_z and $\alpha_\perp$ in Eq. (13)] tend to allow constructive and destructive interference between the individual scattering dipoles. Second, near the center of a parallel plate capacitor, the dipole potential, which is odd in the coordinate parallel to the dipole, tends to integrate
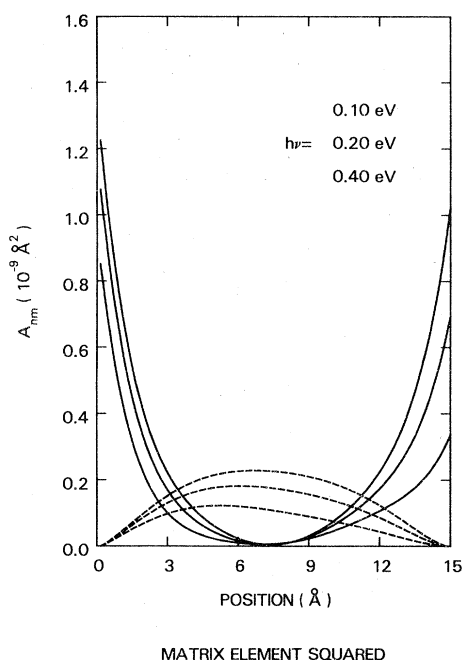
MATRIX ELEMENT SQUARED

FIG. 1. Plots of the angle averaged inelastic tunneling matrix element squared A_{nn11}^k for a single dipole oriented normal (solid line) or parallel (dashed line) to the surface as a function of the position of the dipole relative to the metal electrodes at $z = 0$ Å and $z = 15$ Å, for three different vibrational energy losses. Dipoles oriented normal to the interface have larger inelastic cross sections than dipoles oriented parallel to the interface close to the metal electrodes, but dipoles parallel to the surface are favored deep within the barrier.

to zero for dipoles normal to the interface. This can be seen clearly in Fig. 1, where the incoming and outgoing electron scattering angle averaged coefficient $A_{n,n,1,1}^k$ (dashed line) and $A_{n,n,3,3}^k$ (solid line) [see Eqs. (21) and (22)] are plotted against the position of a point dipole relative to the two metal electrodes (at 0 and 15 Å), for three different vibrational energy losses. This figure shows that for molecules located close to the interfaces, dipoles oriented normal to the surface (A_{nn33}^k) have a higher probability of excitation, but that deep within the oxide, dipoles oriented parallel (A_{nn11}^k) are favored, although at a lower scattering amplitude. Therefore, we expect that the orientation selection rule will depend sensitively on the placement of the dopant molecule with respect to the counter electrode. [Note that in our convention electrons tunnel inelastically from right to left, and the favored bias direction (Al negative) corresponds to a placement of the molecule near $z = 0$.]

Since molecules of experimental interest have spatial extents of several angstroms, a test of orientation selection rules must be made with detailed calculations of a particular molecule of known orientation. Such a molecule is $CH_3SO_3^-$ on alumina.

EXPERIMENTAL DATA

Experimental details of the inelastic tunneling spectra for $CH_3SO_3^-$ have been published elsewhere.[4] The spectrum was taken with an Al-Al$_2$O$_3$-$CH_3SO_3^-$-Pb tunneling junction at 4.2 K, the Pb electrode superconducting, and with approximately 1 mV rms modulation voltage. The resultant vibrational mode energies, normal mode assignments, and measured peak intensities are tabulated in Table I. Analysis of the vibrational mode energies indicates that the SO_3H group bonds to the surface as a sulfonate ion (losing a proton), that the oxygen atoms are bound to the surface in nearly equivalent chemical positions, and there-

TABLE I. $CH_3SO_3^-$ IETS spectrum.

Normal mode number	Symmetry	Description	Intensity (%)[a]	Energy (meV)[b]
1	A_1	ν_s(C–S)	0.079(6)	97.7
2	A_1	ν_s(C–H$_3$)	0.110(6)	362.2
3	A_1	ν_s(S–O$_3^-$)	0.053(6)	128.8
4	A_1	δ_s(C–H$_3$)	0.032(6)	164.5
5	A_1	δ_s(S–O$_3^-$)	0.049(14)	67.9
6	A_2	Torsion		
7a, 7b	E	ρ_a(C–H$_3$)	0.021(14)	119.6
8a, 8b	E	ρ_a(S–O$_3^-$)	0.042(14)	42.5
9a, 9b	E	ν_a(C–H$_3$)	0.082(7)	371.7
10a, 10b	E	ν_a(S–O$_3^-$)	0.062(7)	144.4, 149.4
11a, 11b	E	δ_a(C–H$_3$)	0.039(6)	174.8
12a, 12b	E	δ_a(S–O$_3^-$)	0.014(14)	65.1

[a] Values normalized to percentage of reference conductance at 50 meV, numbers in parentheses are the experimental uncertainty in the preceding digits.

[b] 1 meV = 8.06548 cm^{-1}.

fore that the molecule is oriented with the C–S bond normal to the surface.

The spectrum was taken using standard techniques with a constant current modulation.[2] Under these conditions the ratio of the change in conductance due to the kth vibrational mode divided by the junction conductance at some reference voltage (in our case 50 meV) is given by

$$\Delta\left(\frac{dj}{d(eV)}\right)^k \Big/ (dj/d(eV))_{ref}$$

$$= 4V_\omega^{ref}\int_k dV\, V_{2\omega}/V_\omega^3 \simeq \frac{-4V_\omega^{ref}}{(V_\omega^k)^3}\int_k dV\, V_{2\omega}\,, \quad (24)$$

where V_ω is the amplitude of the first harmonic modulation voltage across the junction, $V_{2\omega}$ is the amplitude of the second harmonic signal, and the integral is taken over the band with the broadly varying background subtracted out. (The integral was taken by cutting out the peaks plotted on chart paper and weighing them.) There was considerable uncertainty in the choice of assumed background. The superconductivity of the Pb electrode helped to resolve the peaks, but also generated uncertainty in peak shapes.[7,8] The error brackets in Table I reflect this uncertainty, which is especially large for small peaks that overlay the background oxide phonons.

MOLECULAR THEORY

The $CH_3SO_3^-$ species has C_{3v} symmetry (see Fig. 2), with 18 normal vibrational modes which are classified according to the following symmetry types:
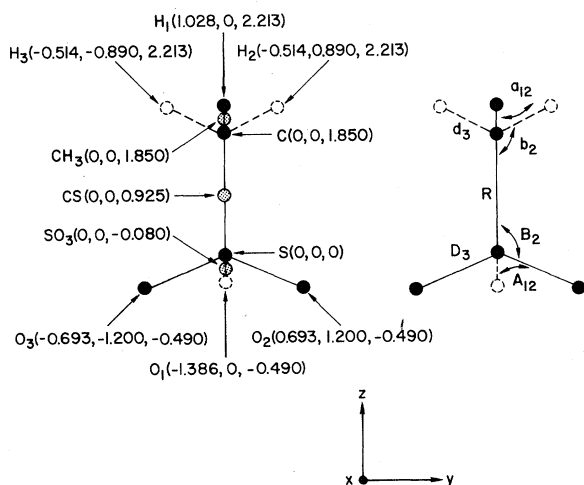

FIG. 2. Geometry, internal coordinates, and the methyl, sulfate, and C–S group positions for the symmetry coordinate sum described in the text, for the $CH_3SO_3^-$ species.

$$\Gamma_{vib} = 5A_1 + A_2 + 6E\,.$$

The A_1 modes (1–5 in Table I) correspond to totally symmetric vibrations with net dipole moments parallel to the C–S axis. The E modes (7–12) correspond to doubly degenerate antisymmetric vibrations with net dipole moments perpendicular to the C–S axis (see Fig. 1, Ref. 4). Both the A_1 and E modes are infrared and Raman active. The A_2 mode corresponds to a torsional vibration about the C–S bond which is forbidden to both infrared and Raman spectroscopies, and has not been observed in IETS.

To compare theory with experiment it is necessary to assign values to $\langle\mu_m^{kl}\rangle$, the expectation value of the dipole moment operator. $\langle\mu_m^{kl}\rangle$ is related to the derivative of the dipole moment with respect to the normal coordinate by

$$\langle\mu_m^{kl}\rangle = \langle Q_k\rangle_{01}\frac{\partial\mu_m^l}{\partial Q_k}\,, \quad (25)$$

where $\langle Q_k\rangle_{01}$ is the expectation value of the kth normal coordinate between the ground and first excited states (our measurements were made at a temperature such that $\hbar\omega_k \gg kT$) and μ_m^l is the lth Cartesian component of the dipole moment due to the mth bond. The connection between normal coordinates Q and symmetry coordinates S, for which dipole derivatives are traditionally tabulated, is made through a normal coordinate analysis and the L matrix[9]

$$\frac{\partial\mu_m^l}{\partial Q_k} = \sum_j L_{kj}\frac{\partial\mu_m^l}{\partial S_j}\,. \quad (26)$$

Then

$$\langle\mu_m^{kl}\rangle = \sum_j A_{kj}\frac{\partial\mu_m^l}{\partial S_j}\,, \quad (27)$$

where

$$A_{kj} \equiv \langle Q_k\rangle_{01}L_{kj}\,. \quad (28)$$

We obtained the amplitudes A_{kj} of the jth symmetry coordinate for the kth normal mode using the following information: The symmetry coordinates in terms of the internal coordinates shown in Fig. 2 are given in Table II. Bürger, Burcsyk, and Blaschette[10] performed a normal mode coordinate analysis using these symmetry coordinates. Assuming a staggered molecular geometry, they calculated the force-constant matrix F by using the G matrix of Clark and Weber[11] and solving the secular equation

$$|GF - E\omega_k^2| = 0\,, \quad (29)$$

where E is the unit matrix.

The secular equation defines a set of simultaneous equations by matrix multiplication

TABLE II. Symmetry coordinates of $CH_3SO_3^-$.

			Approximate mode description[a]	
A_1 species	$S_1 = R$ [b]		1	$\nu_a(C-S)$
	$S_2 = (d_1 + d_2 + d_3)/3^{\frac{1}{2}}$		2	$\nu_s(C-X_3)$
	$S_3 = (D_1 + D_2 + D_3)/3^{\frac{1}{2}}$		3	$\nu_s(S-O_3^-)$
	$S_4 = (a_{12} + a_{13} + a_{23} - b_{12} - b_{13} - b_{23})/6^{\frac{1}{2}}$		4	$\delta_s(C-X_3)$
	$S_5 = (A_{12} + A_{13} + A_{23} - B_{12} - B_{13} - B_{23})/6^{\frac{1}{2}}$		5	$\delta_s(S-O_3^-)$
E species (doubly degenerate)	$S_{7a} = (2b_1 - b_2 - b_3)/6^{\frac{1}{2}}$	$S_{7b} = (b_2 - b_3)/2^{\frac{1}{2}}$	7	$\rho_a(C-X_3)$
	$S_{8a} = (2B_1 - B_2 - B_3)6^{\frac{1}{2}}$	$S_{8b} = (B_2 - B_3)/2^{\frac{1}{2}}$	8	$\rho_a(S-O_3^-)$
	$S_{9a} = (2d_1 - d_2 - d_3)/6^{\frac{1}{2}}$	$S_{9b} = (d_2 - d_3)/2^{\frac{1}{2}}$	9	$\nu_a(C-X_3)$
	$S_{10a} = (2D_1 - D_2 - D_3)/6^{\frac{1}{2}}$	$S_{10b} = (D_2 - D_3)/2^{\frac{1}{2}}$	10	$\nu_a(S-O_3^-)$
	$S_{11a} = (2a_{23} - a_{31} - a_{12})/6^{\frac{1}{2}}$	$S_{11b} = (a_{31} - a_{23})/2^{\frac{1}{2}}$	11	$\delta_a(C-X_3)$
	$S_{12a} = (2A_{23} - A_{31} - A_{12})/6^{\frac{1}{2}}$	$S_{12b} = (A_{31} - A_{23})/2^{\frac{1}{2}}$	12	$\delta_a(S-O_3^-)$

[a] There is considerable coupling among A_1, species for modes 1–5, and among E species for modes 7–12 (see Table III).

[b] The variables here refer to changes in internal coordinates in Fig. 3.

$$(GF - E\omega_k^2)A_{kj} = 0 . \tag{30}$$

We found the absolute values of A_{kj} by first solving Eq. (30) for the relative values of A_{kj} and then equating the potential energy of the amplitudes to that of the expectation value of the normal coordinate $\langle Q_k\rangle_{01}$ between the ground and first excited state of a linear harmonic oscillator[9]:

$$\frac{1}{2}\sum_{ij} F_{ij}A_{ki}A_{kj} = \frac{1}{2}\omega_k^2\langle Q_k\rangle_{01}^2 , \tag{31}$$

where

$$\langle Q_k\rangle_{01} = \int \psi_1^* Q_k \psi_0 dQ_k = (\hbar/2\omega_k)^{1/2} . \tag{32}$$

Table III shows the computed values of A_{kj} for $CH_3SO_3^-$. For this application we cast the atom-by-atom sum for the tunneling electron-molecule interaction [Eq. (6)] into a symmetry coordinate sum

$$V_I = -e\sum_j \vec{\mu}_j^k \cdot \vec{\nabla}_j\left(\frac{1}{|\vec{r} - \vec{R}_j^0|}\right)e^{i\omega_k t} , \tag{33}$$

where j is the symmetry coordinate number and $\vec{R}_j^0$ is the center position assigned to the jth symmetry coordinate. This makes direct comparison with infrared symmetry coordinate dipole moment derivatives quite straightforward. We found that the qualitative results we obtained from the theory were the same (for a given net dipole derivative with respect to symmetry coordinate) whether we cast our potential in an atom-by-atom, bond-by-bond, or symmetry coordinate sum. This is a result both of the long-range nature of the interaction and the relatively small size of the molecule. We assumed $\vec{R}_j^0$ to be at the center of the methyl group

TABLE III. $CH_3SO_3^-$ symmetry coordinate amplitudes A_{kj}. k and j refer, respectively, to normal mode number and symmetry coordinate number.

k/j	1	2	3	4	5	
1	0.041 77	0.000 34	0.008 58	0.015 19	0.027 55	
2	−0.003 77	0.076 58	0.000 01	−0.009 20	0.000 00	
3	−0.014 70	0.000 08	0.033 30	0.017 25	−0.020 47	
4	0.013 82	0.001 82	−0.003 60	0.172 87	−0.000 86	
5	−0.020 04	−0.000 37	0.002 62	0.012 00	0.069 81	
k/j	$7a, 7b$	$8a, 8b$	$9a, 9b$	$10a, 10b$	$11a, 11b$	$12a, 12b$
$7a, 7b$	0.122 02	0.013 52	−0.003 40	0.006 92	−0.046 60	−0.000 32
$8a, 8b$	−0.025 02	0.078 78	0.000 24	0.001 75	0.010 00	0.014 27
$9a, 9b$	−0.006 19	−0.004 24	0.078 48	−0.000 08	0.007 10	0.000 00
$10a, 10b$	−0.022 56	−0.015 60	0.000 90	0.037 89	0.009 96	0.019 22
$11a, 11b$	0.048 16	−0.003 56	0.002 86	−0.000 90	0.173 94	−0.000 70
$12a, 12b$	0.013 58	−0.007 36	−0.000 52	−0.009 50	−0.004 82	0.071 93

TABLE IV. Comparison of methyl group dipole derivatives $\partial\mu/\partial S_j$ expressed in electron units. $e = 4.803\ D/\mathrm{\mathring{A}}$; the absolute values are important, sign differences often result from different choices of $\partial\mu/\partial Q_i$ phase and coordinate systems.

j	mode	CH_3F^a	CH_3Cl^a	CH_3Br^a	CH_3I^a	CH_3CCH^b	$CH_3CH_3{}^c$	$CH_3CH_2CH_3{}^d$	$CH_3SO_3{}^-$ $C-S_\perp{}^e$	$CH_3SO_3{}^-$ $C-S_\parallel$
2	ν_s	0.118	0.123	0.118	0.099	−0.125	0.162	−0.156(−0.019)	−0.187(6)	−0.382(10)
4	β_s	0.030	0.050	−0.068	0.101	−0.019	0.030	0.036(0.035)	−0.034(4)	−0.075(9)
7	ρ_a	0.001	−0.029	−0.050	−0.063	−0.050	−0.035	−0.040(0.022)	−0.080(20)	−0.046(13)
9	ν_a	0.156	0.048	0.033	0.020	−0.077	−0.180	−0.183(−0.004)	0.231(7)	0.139(5)
11a	β_a	−0.057	−0.059	−0.054	−0.048	0.080	0.046	0.038(−0.013)	−0.050(1)	−0.029(1)
9b	β_a	0.001	−0.029	−0.050	−0.063	−0.050	−0.035	−0.014	−0.080(20)	−0.046(13)
9b	ν_a	0.156	0.048	0.033	0.020	−0.077	−0.180	−0.168	0.231(7)	0.139(5)
11b	β_a	−0.057	−0.059	−0.054	−0.048	0.080	0.046	0.041	0.050(1)	−0.029(1)

[a] Values from Ref. 12 with signs (+−−, +−−) for $\partial\mu/\partial Q_i$ from Ref. 13; these values are reportedly improvements over previous values in Ref. 14.

[b] Values from Ref. 15.

[c] Values from Ref. 16; values are reportedly improvements over previous values in Refs. 17 and 18.

[d] Values from Ref. 17; values in parentheses are components perpendicular to CX axis and result from collapse of axial symmetry in molecule.

[e] $\partial\mu/\partial S_j$ for $j = 1,\ 3,\ 5,\ 8,\ 10,$ and 12 are, respectively, −0.102, −0.589, −0.193, −0.104, 0.204, and −0.035.

(see Fig. 2) for symmetry coordinates 2, 4, 7, 9, and 11, vibrations of the C–H bonds, $\vec{R}_j^0$ at the center of the $SO_3{}^-$ group for coordinates 3, 5, 8, 10, and 12, vibrations of the S–O bonds, and $\vec{R}_j^0$ at the center of the C–S bond for symmetry coordinate 1, the C–S stretching mode. We inserted a set of known or to-be-fit dipole derivatives $\partial\mu/\partial S_j$ into Eq. (27), then calculated intensities using Eq. (21).

RESULTS AND DISCUSSION

Unfortunately no complete analysis for the derivatives $\partial\mu/\partial S_j$ exists for the $CH_3SO_3{}^-$ species. However, dipole derivatives have been obtained (from infrared spectra and the theory of infrared intensities) for the CH_3 groups of a number of similar species. Table IV shows the total dipole moment derivatives with respect to symmetry coordinates of the CH_3 groups in CH_3X (X = F, Cl, Br, I, CCH, CH_3, and C_2H_5). One might expect the dipole derivatives for halogen substituted methanes CH_3X to be significantly different than those for $CH_3SO_3{}^-$, not only because of the nontetrahedral structure of the substituted group (X), but also because of the highly polarized character of the C–X bond.

Using the same arguments, one might expect the methyl ligand dipole derivatives to be most similar to $CH_3SO_3{}^-$ for ethane (CH_3CH_3) and propane ($CH_3CH_2CH_3$), both of which have a tetrahedral X-bonding structure and nonpolar C–C bond. In fact, we will compare IETS results mostly with the ethane (CH_3CH_3) dipole derivatives in what is to follow.

If the $CH_3SO_3{}^-$ ions have the orientation proposed by Hall and Hansma, e.g., with the C–S bond nor-

mal to the oxide, our theory would predict that the intensities of the antisymmetric modes (with net dipole moments parallel to the oxide) should be reduced relative to the intensities of the symmetric modes. The quantitative reduction depends, however, rather sensitively on the effective charge-to-image plane distance, as pointed out above (Fig. 1). We compare in Fig. 3 experimental and theoretical intensities for the methyl group vibrations (modes 2, 4, 7, 9, and 11) assuming infrared-derived ethane dipole derivatives and the C–S bond normal to the interface, for three different hydrogen atom-image plane distances d. Note that as d increases the symmetric modes numbers 2 and 4 become weaker while the antisymmetric modes 7, 9, and 11 become stronger. The best fit between theory and experiment occurs at $d = 1.5$ Å, although theory predicts in all cases a symmetric C–H bond mode no. 4 too large and its corresponding antisymmetric mode no. 11 too small.

If, on the other hand, we assume a molecular orientation with the C–S bond parallel to the oxide, the agreement between theory and experiment is poor for all assumed d's. Figure 4 compares predictions for normal orientation versus parallel orientation for $d = 1.5$ Å with experiment. The better fit of theory to experiment for normal orientation supports the proposed orientation of Hall and Hansma.

These conclusions are not qualitatively changed if we use the infrared-derived dipole derivatives of the CH_3 groups in propane $CH_3CH_2CH_3$. In order to give some idea of the range of predicted IETS intensities, we show in Fig. 5 experiment and theory for infrared-derived dipole derivatives of
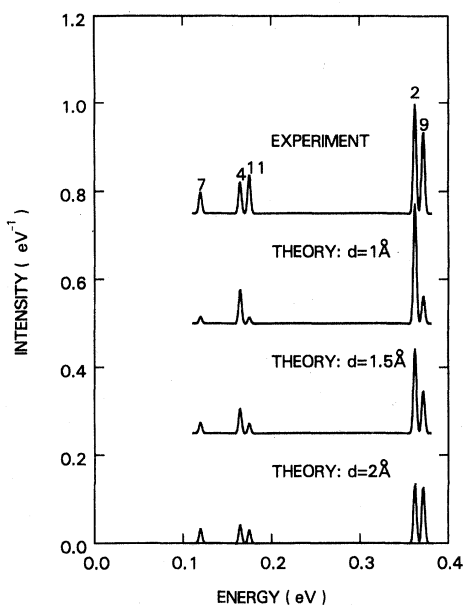
FIG. 3. Experimental versus theoretical predictions for the methyl group intensities assuming infrared-derived ethane dipole derivatives, the C–S bond oriented normal to the interface for three different spacings d between the hydrogen atoms and the Pb effective image plane. As the molecule is moved away from the interface, the modes with net dipole moments normal to the interface (nos. 2 and 4) become weaker and the modes parallel to the interface (nos. 4, 7, and 11) become stronger.
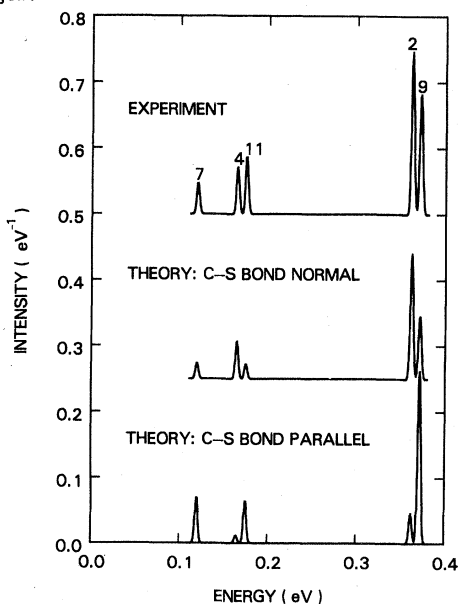

FIG. 4. Comparison of experiment with theoretical predictions for the methyl group intensities, assuming infrared-derived ethane dipole derivatives, an effective nearest-hydrogen to Pb image-plane distance of 1.5 Å, for the C–S bond normal versus parallel to the interface. The better agreement for C–S normal supports the proposed orientation of Hall and Hansma.
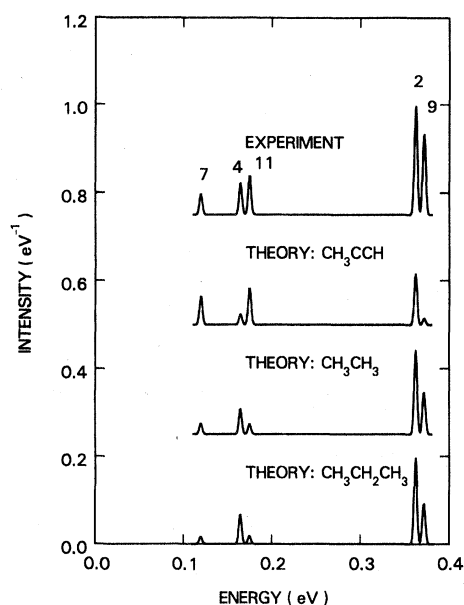

FIG. 5. Comparison of experiment with theoretical predictions for the methyl group intensities assuming the C–S bond normal to the interface, a hydrogen to Pb image-plane distance of 1.5 Å for infrared derived dipole derivatives from CH_3X, where X = CCH, CH_3, and CH_2CH_3.

CH_3CCH, CH_3CH_3, and $CH_3CH_2CH_3$ for the C–S bond normal to the surface and hydrogen-Pb image plane distance of 1.5 Å. Note that if one uses the dipole derivatives of methyl acetylene (CH_3CCH) the relative intensities of modes nos. 4 and 11 are reversed to more nearly agree with the tunneling results, indicating that relative intensities of these mode intensities are sensitive to the type of chemical bonding to the methyl group carbon.

We can also work backwards from IETS intensities to molecular dipole derivatives. Table IV includes the vibrational mode dipole derivatives obtained using a nonlinear least-squares fit of the 11 dipole derivatives $\partial\mu/\partial S_j$ to the 11 measured IETS intensities, assuming $d = 1.5$ Å and the C–S bond normal to the oxide. We estimated the error in the IETS dipole derivatives by making the least-squares fit for the minimum and maximum (one standard deviation) intensities for all of the measured peaks. These estimated errors appear in parentheses in Table IV. The agreement in Table IV between the IETS dipole derivatives for $CH_3SO_3^-$ and the infrared dipole derivatives for CH_3CH_3 and $CH_3CH_2CH_3$ is good.

Also included in Table IV are the best-fit values for an assumed orientation with the C–S bond parallel to the interface. In this case the qualitative agreement to the other species is poor. In particular, $\partial\mu/\partial S_2$ is very large, well outside the range of the error bars. The much better agreement be-

tween the IETS and ir results for the C–S bond normal rather than parallel to the interface, supports the orientation proposed by Hall and Hansma for $CH_3SO_3^-$.

This is the first attempt to unravel the information contained in all the intensities of the IETS of a simple molecule. We have attempted to compare the dipole derivatives of ethane and propane to $CH_3SO_3^-$. It is remarkable that there is such good agreement, especially when one considers the following problems:

(1) We are comparing different molecules in different environments. For a truly quantitative test we would need to know the ir dipole derivatives of $CH_3SO_3^-$ chemisorbed on alumina, for there may be significant surface effects.[19]

(2) Our theory ignores any polarizability interactions. We might expect our best-fit dipole derivatives to be higher than the ir values in order to compensate.

(3) Finally, in our simple model we assumed the positions of the dipoles in the molecule. Although our interaction potential is long range, it is sensitive to the position of the dipole relative to the nearby electrode. The real positions may well be different than we assumed.

CONCLUSIONS

A detailed application of an effective dipole transfer Hamiltonian theory to vibrational mode intensities in IETS supports the proposed orientation for $CH_3SO_3^-$ on alumina and gives reasonably good agreement between dipole derivatives fit to IETS data and values obtained from infrared experiments. One can infer molecular orientations from such an analysis of IETS intensities.

ACKNOWLEDGMENTS

[1]R. C. Jaklevic and J. Lambe, Phys. Rev. Lett. 17, 1139 (1967); Phys. Rev. 165, 821 (1968); recent surveys are contained in Ref. 2.

[2]P. K. Hansma, Phys. Rep. 30C, 146 (1977); *Inelastic Electron Tunneling Spectroscopy*, edited by T. Wolfram (Springer, Berlin, 1978); W. H. Weinberg, Annu. Rev. Phys. Chem. 29, 115 (1978); R. G. Keil *et al.*, Appl. Spectrosc. 30, 1 (1976); P. K. Hansma and J. Kirtley, Acc. Chem. Res. 11, 440 (1978).

[3]John Kirtley, D. J. Scalapino, and P. K. Hansma, Phys. Rev. B 14, 3177 (1976).

[4]J. T. Hall and P. K. Hansma, Surf. Sci. 71, 1 (1978).

[5]M. F. Muldoon, R. A. Dragoset, and R. V. Coleman, Phys. Rev. B 20, 416 (1979).

[6]John Kirtley and Paul Soven, Phys. Rev. B 19, 1812 (1979).

[7]R. Magno and J. G. Adler, J. Appl. Phys. 49, 5571 (1978).

[8]John Kirtley and Paul K. Hansma, Phys. Rev. B 13, 2910 (1976).

[9]E. B. Wilson Jr., J. C. Decius, and P. C. Cross, *Molecular Vibrations* (McGraw-Hill, New York, 1955).

[10]H. Burger, K. Burczyk, and A. Blaschette, Monatsh. Chem. 101, 102 (1970).

[11]E. A. Clark and A. Weber, J. Chem. Phys. 45, 1759 (1966).

[12]J. W. Russel, C. D. Needham, and J. Overend, J. Chem. Phys. 45, 3383 (1966).

[13]J. H. Newton and W. B. Person, J. Chem. Phys. 64, 3036 (1976).

[14]A. D. Dickson, J. M. Mills, and B. Crawford, Jr., J. Chem. Phys. 27, 445 (1957).

[15]S. Kardo and Y. Koga, J. Chem. Phys. 69, 4022 (1978).

[16]G. Jalsovszky and P. Pulay, J. Mol. Struct. 26, 277 (1975).

[17]S. Kardo and S. Saeki, Spectrochim. Acta 29A, 735 (1973).

[18]I. M. Nyquist, I. M. Mills, W. B. Person, and B. Crawford, Jr., J. Chem. Phys. 26, 552 (1956).

[19]L. H. Little, *Infrared Spectra of Absorbed Species* (Academic, New York, 1966), Chap. 15.